

Visible Range Plasmonic Modes on Topological Insulator Nanostructures

Alexander M. Dubrovkin,* Giorgio Adamo, Jun Yin, Lan Wang, Cesare Soci, Qi Jie Wang, and Nikolay I. Zheludev*

Surface plasmons are electromagnetic excitations existing at the interface between dielectrics and conductive media, where confined oscillations of electromagnetic fields are coupled to oscillations of free electrons.^[1] They are the key to nanophotonic applications such as light-harvesting, biological sensing, ultra-compact interchip interconnects, and all-optical data processing chips. Noble metals such as silver, gold, and copper as well as aluminum support localized and propagating plasmonic excitation. Highly doped semiconductors, transparent conductive oxides, perovskites, metal nitrides, silicides, germanides,^[2] and recently discovered 2D materials,^[3] such as graphene,^[4] have been suggested as new plasmonic materials beyond conventional metals.

Recently, topological insulators (TIs)^[5] have been reported as novel plasmonic medium.^[6–12] Visible range localized plasmons were detected in chalcogenide crystals via reflection and cathodo-luminescent spectra^[6,7] and by energy loss spectroscopy.^[8,9] Ellipsometry data^[6] and theoretical calculations^[8] in these studies indicate that the plasmons observed in the visible range may include a contribution from strong spin-orbit coupling inducing metal-like surface layers, in addition to the bulk optical conductivity given by interband transitions in the medium. Topological insulators demonstrate tunability of

plasmon resonances in the entire visible spectrum by varying the partial ratio of the building elements in TI compounds,^[9,13] bearing high potential for photonics applications. Recent studies revealed potential benefits of using TI visible range plasmons for light harvesting applications.^[7,9] TIs form an intrinsic core-shell structure with metal-like surface state layer and insulating bulk, while its practical applications in optical or electronic devices require low residual conductivity of the bulk.^[7] $\text{Bi}_{2-x}\text{Sb}_x\text{Te}_{3-y}\text{Se}_y$ topological insulators show well pronounced surface dominated electronic transport and highly insulating bulk interior,^[5,14] compared to simpler and more studied compounds such as Bi_2Se_3 , Bi_2Te_3 , Sb_2Te_3 .^[5]

In this work, we report first near-field optical observations of visible range plasmons in $\text{Bi}_{1.5}\text{Sb}_{0.5}\text{Te}_{1.8}\text{Se}_{1.2}$ (BSTS)^[6,14–16] nano- and microstructures. By using scattering-type technique we accessed both, the amplitude and the phase of the plasmons field, and revealed dipolar and higher-order plasmon modes on artificially carved nanostructures and naturally exfoliated flakes.

BSTS was synthesized from high-purity Bi, Sb, Te, and Se by modified Bridgman method as in our previous works.^[6,14] The resulting material forms high quality single crystals, which were mechanically exfoliated on commercial thermally oxidized silicon substrate (285 nm of SiO_2). This method allows easy fabrication of the TI micro- and nanoflakes with typical thicknesses ranging from few to several hundred nm. We investigate both naturally occurring flakes, following exfoliation, and artificially fabricated nanostructures, carved by further focused ion beam (FIB) milling of the flakes (see details in Supporting Information). All samples were capped with 5 nm of SiO_2 to prevent the TI from atmosphere exposure. The capping has been realized by physical vapor deposition in high vacuum (3×10^{-7} mbar), while the sample was attached to water-cooled holder.

For experimental imaging of TI plasmons, we use polarization sensitive scattering-type scanning near-field optical microscope (s-SNOM)^[17] operating at wavelength of 633 nm. s-SNOM is based on Neaspec commercial instrument which we upgraded with a balanced detection. To excite/detect localized plasmons in BSTS, we elaborate sp-geometry scheme^[18] for measurements (see sketch of the experiment in **Figure 1a**). Here the sample is illuminated in oblique configuration with s-polarized cw laser radiation. The incident laser beam excites electromagnetic oscillations in the TI nanostructure, which are mapped by recording s-SNOM tip-scattered signal at each point of the scan. P-polarized component of the scattered light is selected by a polarizer placed in front of the detector. Pseudoheterodyne interferometric detection at nonlinear harmonics of the tip tapping frequency (fourth and third in this work)^[19] allows us to measure amplitude and phase of the scattered

Dr. A. M. Dubrovkin, Dr. G. Adamo, Prof. C. Soci,
Prof. Q. J. Wang, Prof. N. I. Zheludev
Centre for Disruptive Photonic Technologies
TPI

Nanyang Technological University
637371 Singapore
E-mail: dubrovkin@ntu.edu.sg; niz@orc.soton.ac.uk

Dr. A. M. Dubrovkin, Dr. G. Adamo, Dr. J. Yin,
Prof. C. Soci, Prof. Q. J. Wang, Prof. N. I. Zheludev
School of Physical and Mathematical Sciences
Nanyang Technological University
637371 Singapore

Prof. L. Wang
RMIT University
Department of Physics
School of Applied Sciences
Melbourne, VIC 3000, Australia

Prof. Q. J. Wang
Centre for OptoElectronics and Biophotonics
School of Electrical and Electronic Engineering
Nanyang Technological University
639798 Singapore

Prof. N. I. Zheludev
Optoelectronics Research Centre and Centre for Photonic Metamaterials
University of Southampton
SO17 1BJ, UK



DOI: 10.1002/adom.201600768

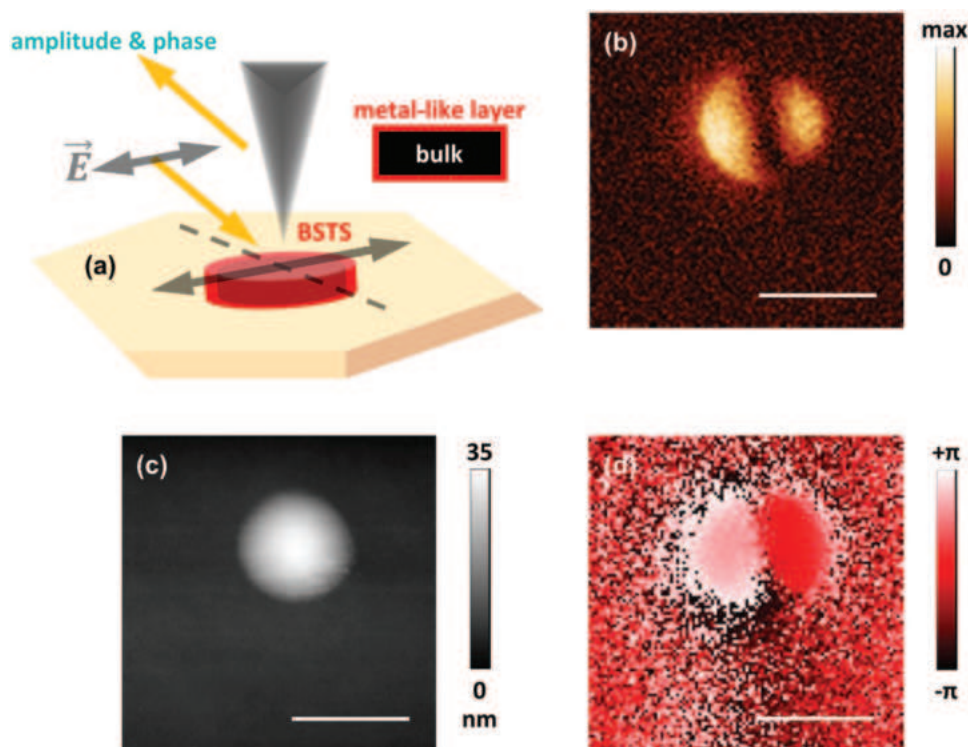


Figure 1. a) Sketch of the scattering-type scanning near-field optical microscopy experiment, realized in sp-geometry (s-polarization excitation, p-polarization detection). This configuration is used for localized plasmon mapping. b,d) Near-field amplitude and phase images of BSTS nanodisk fabricated at Si-SiO₂ substrate by FIB milling. c) Topography of the disk, recorded by s-SNOM. The excitation wavelength is 633 nm. Scale bars are 150 nm.

signal, which are proportional to those of the surface plasmon field around the TI structures.

Near-field images of BSTS nanodisk with 150 nm diameter, recorded at $\lambda = 633$ nm, are shown in Figure 1b,d. Amplitude distribution (Figure 1b) of the plasmon field features two well defined maxima, which oscillate in time with opposite phase (Figure 1d). This is a typical picture of dipolar localized surface plasmon mode excitation.^[18,20] The disk was FIB milled from a large TI flake on top of a SiO₂ slab, such that the surrounding flake is completely milled away. We observed dipole modes in FIB-fabricated nanostructures of different shape (e.g., rods, etc.), size, and thickness. Measurements show that these geometrical parameters affect the dipole field enhancement and the corresponding phase contrast. Plasmon modes have also been detected in TI nanodisks fabricated on top of optically thick TI crystals.

As a next step, we study TI nanoflakes made by exfoliation, which produces high-quality samples. We observe a plasmon response for flakes with thickness down to 13 nm. An example is shown in Figure 2. The nanoflake of about 150 nm width and 13 nm thickness has been excited with the polarization orthogonal to its long axis. The near-field image (Figure 2b) taken at $\lambda = 633$ nm shows the formation of stripe-shaped maxima in the amplitude distribution at the edges of the flake. The mode elongation is a direct consequence of the flake geometry. The observed phase distribution (Figure 2c) is qualitatively similar to the one presented in Figure 1d and shows a dipolar mode excitation. We found that the experimentally measured field amplitude and phase data agree qualitatively with the

numerical modeling (Figure 2e,f), conducted by full-wave 3D Maxwell solver COMSOL. The shape and size of the TI flake has been designed using the experimentally measured one; the optical permittivities of the TI used in the numerical simulations are the ones obtained by ellipsometric measurement in our previous work.^[6] As it can be seen from Figure 2d, the field amplitude is concentrated near the edges of the flake, which is expected in a plasmonic medium.

Finally, we report higher order plasmon modes excitation on larger BSTS flakes prepared by exfoliation. Near-field amplitude image of the flake of ≈ 55 nm thicknesses is presented in Figure 3a. It features three peaks in the field distribution. The polarization of the incident radiation ($\lambda = 633$ nm) is orthogonal to the long axis of the flake. We observe a higher order mode phase distribution, accompanying field amplitude features, which is an alternating sequence of phase and antiphase (Figure 3b). Influence of the s-SNOM tip type (metallic or dielectric) on the recorded mode shape was negligible as could be seen from comparison of images Figure 3a (taken with a metal-coated tip) and Figure 3d (taken with a dielectric tip). We note that for dipole mode in Figure 1 a metallic tip was used, while measurements with a dielectric tip showed similar data of lower intensity; for the dipole mode in Figure 2 a dielectric tip was used.

The origin of surface plasmons should be attributed to the negative value of dielectric permittivity (real part, ϵ') of the BSTS topological insulator which was experimentally measured by spectroscopic ellipsometry. The experimental data (Figure 4, pink points) show that ϵ' of BSTS crystals has negative values

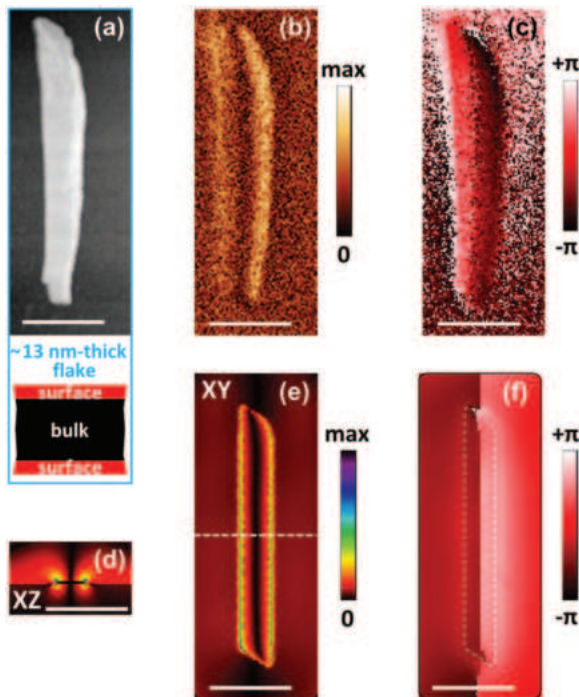


Figure 2. a) Topography of thin BSTS nanoflake fabricated by mechanical exfoliation on Si-SiO₂; layout of the flake cross-section. b,c) Near-field amplitude and phase images recorded at $\lambda = 633$ nm. d) Numerical simulation of the field amplitude in the vertical cross section, taken in the center of the flake. e,f) Numerical simulation of the field amplitude and phase in the lateral plane, 1 nm above the flake. Scale bars are 400 nm.

in the spectral interval between 200 and 670 nm,^[6] which includes the 633 nm laser wavelength used in our s-SNOM measurements. The origin of the plasmonic behavior of TIs across a very broad spectral range is object of intense research

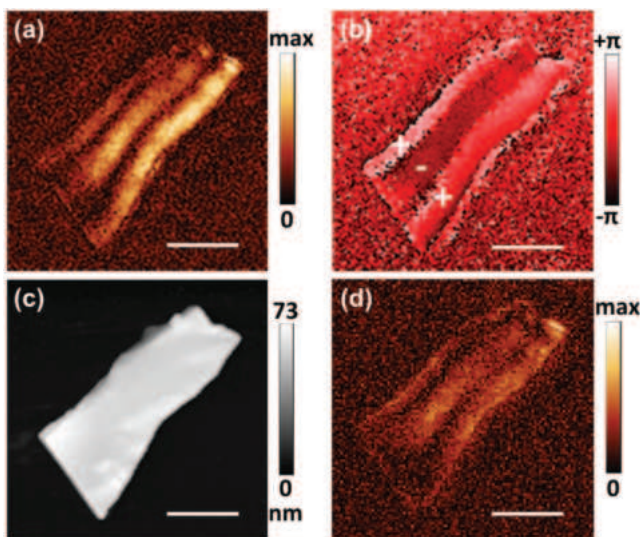


Figure 3. a,b) Near-field amplitude and phase images of higher order plasmon mode recorded at $\lambda = 633$ nm with metal-coated tip in BSTS flake. c) Topography of the flake at Si-SiO₂ substrate. d) Near-field amplitude data recorded with dielectric tip. Scale bars are 800 nm.

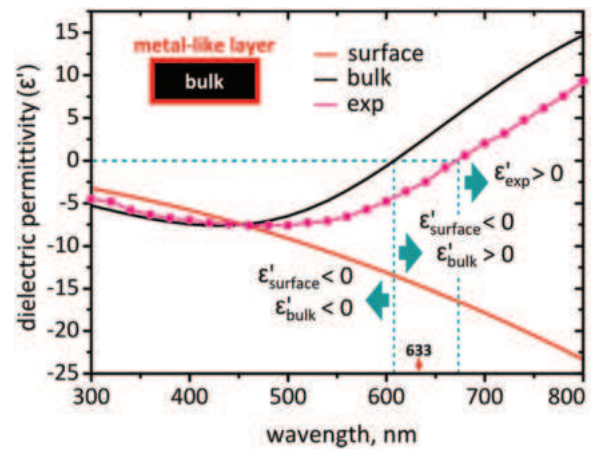


Figure 4. Dielectric permittivity (real part) of BSTS crystal: experimental data obtained by ellipsometry (marked with pink); data for the metal-like surface layer (red curve) and the bulk (black curve), combination of which consistently fits experimental points (data are taken from Ou et al.^[6]).

activity in recent years.^[6–12,21] The analysis of the ellipsometry data of our BSTS TI crystals showed that the dielectric permittivity could not be consistently fitted with a single-layer model of a semiconductor material (represented by Tauc-Lorentz dispersion formula^[22]) suggesting that a two-layers model, which treated the TI as a combination of the semiconductive bulk and a metal-like surface layer with 3D Drude-like dispersion, may be instead used to appropriately describe the experimental permittivity values. The ellipsometric fitting showed quantitatively that in the spectral interval between 200 and 608 nm both bulk and surface contribute to the plasmonic response due to their negative permittivities, ϵ'_{bulk} and $\epsilon'_{\text{surface}}$ (Figure 4, black and red curves), while beyond 608 nm the bulk should be considered as a lossy dielectric.

Two-layers description of TIs is in agreement with our recent first-principle density functional theory (DFT) modeling.^[13] The DFT calculations of the electronic band structure and the dielectric functions of Bi_{2-x}Sb_xTe_{3-y}Se_y slabs of various composition have identified the interplay between contributions of the bulk negative permittivity and the metal-like surface to the optical response of TI compounds at visible range frequencies. Our calculations show that with account of spin-orbit coupling additional charge density responsible for DC and optical conductivity of surface layer accumulates within two to three quintuple layers from the surface (≈ 2.5 – 3.5 nm). Here carriers have nonzero masses and the two-dimensional models used to describe plasmonic response in graphene with massless electrons and Dirac dispersion are not suitable for the description of the optical response. We found that conventional three-dimensional Drude model of the surface layer (plasma frequency $\omega_p = 4.49$ eV) superimposed with the optical response due to interband transitions well fits experimental data for Bi_{2-x}Sb_xTe_{3-y}Se_y. This picture is further supported by independent determination of ultraviolet plasma frequency of chalcogenide TI crystal Bi₂Se₃ by electron energy-loss spectroscopy ($\omega_p = 5.5$ eV).^[23]

The described two-layers model implies that a BSTS flake's interior should not contribute to the plasmon mode at $\lambda = 633$ nm due to the positive value of ϵ'_{bulk} , while overall

effective dielectric permittivity ϵ' originating the plasmon response is negative as a result of metal-like layer contribution. We note that some low-loss medium with a positive ϵ' in the visible range, such as silicon, may still support sufficiently strong localized modes of nonplasmonic nature for nanostructures of large thickness.^[24] We argue, that in our experiments, the bulk part of BSTS flakes with the positive ϵ'_{bulk} is not responsible for dipole features due to a very small flakes thickness and sufficiently large losses in the bulk.^[6] A vertical cross-section of the flake is schematically illustrated in the bottom part of Figure 2a. As an example, the 13 nm thick flake treated in the two-layers model should consist of top surface layer (≈ 1.5 nm according to Ou et al.^[6]), bulk (≈ 10 nm) and bottom surface layer (≈ 1.5 nm) which gives the surface/bulk geometrical ratio of $\approx 3:10$. At the same time, conductivity of the metal-like layer is much higher than residual conductivity of the insulating bulk (e.g., $\approx 99\%$ surface electronic transport contribution can be realized in 200 nm thick BSTS nanoflake devices^[14]), and the optical losses of the surface layer are much smaller than of the bulk interior.^[6]

In summary, we have presented first direct near-field observations of the visible range plasmon excitation in BSTS topological insulator.^[25] Scattering-type near-field microscopy of the TI nanostructures revealed dipolar and higher-order plasmon modes with well-defined field amplitude and phase profiles. Experimental data are supported by full-wave electromagnetic numerical simulations and corroborated with the two-layer model of TIs of the BSTS family.

Supporting Information

Supporting Information is available from the Wiley Online Library or from the author.

Following a period of embargo, the data from this paper can be obtained from the University of Southampton ePrints research repository, <http://dx.doi.org/10.5258/SOTON/400746>.

Acknowledgements

The authors acknowledge the support of the Singapore MOE Grants MOE2011-T3-1-005 and MOE Tier 1 M401040000, EPSRC (U.K.) grant EP/M009122/1 and Australian Research Council, ARC Centre of Excellence-FLEET. The authors thank Azat Sulaev for growth of $\text{Bi}_{1.5}\text{Sb}_{0.5}\text{Te}_{1.8}\text{Se}_{1.2}$ crystals.

Received: September 21, 2016

Published online:

- [1] S. A. Maier, *Plasmonics: Fundamentals and Applications*, Springer Science + Business Media, New York **2007**.
- [2] a) A. J. Hoffman, L. Alekseyev, S. S. Howard, K. J. Franz, D. Wasserman, V. A. Podolskiy, E. E. Narimanov, D. L. Sivco, C. Gmachl, *Nat. Mater.* **2007**, *6*, 946; b) P. R. West, S. Ishii, G. V. Naik, N. K. Emani, V. M. Shalaev, A. Boltasseva, *Laser Photonics Rev.* **2010**, *4*, 795; c) M. A. Noginov, L. Gu, J. Livenere, G. Zhu, A. K. Pradhan, R. Mundle, M. Bahoura, Yu. A. Barnakov, V. A. Podolskiy, *Appl. Phys. Lett.* **2011**, *99*, 021101; d) G. V. Naik, J. Kim, A. Boltasseva, *Opt. Mater. Express* **2011**, *1*, 1090.
- [3] T. Stauber, *J. Phys.: Condens. Matter* **2014**, *26*, 123201.
- [4] T. Low, P. Avouris, *ACS Nano* **2014**, *8*, 1086.
- [5] Y. Ando, *J. Phys. Soc. Jpn.* **2013**, *82*, 102001.
- [6] J. Y. Ou, J. K. So, G. Adamo, A. Sulaev, L. Wang, N. I. Zheludev, *Nat. Commun.* **2014**, *5*, 5139.
- [7] Z. Yue, B. Cai, L. Wang, X. Wang, M. Gu, *Sci. Adv.* **2016**, *2*, e1501536.
- [8] M. Zhao, M. Bosman, M. Danesh, M. Zeng, P. Song, Y. Darma, A. Rusydi, H. Lin, C.-W. Qiu, K. P. Loh, *Nano Lett.* **2015**, *15*, 8331.
- [9] M. Zhao, J. Zhang, N. Gao, P. Song, M. Bosman, B. Peng, B. Sun, C.-W. Qiu, Q.-H. Xu, Q. Bao, K. P. Loh, *Adv. Mater.* **2016**, *28*, 3138.
- [10] P. Di Pietro, M. Ortolani, O. Limaj, A. Di Gaspare, V. Giliberti, F. Giorgianni, M. Brahlek, N. Bansal, N. Koirala, S. Oh, P. Calvani, S. Lupi, *Nat. Nanotechnol.* **2013**, *8*, 556.
- [11] M. Autore, H. Engelkamp, F. D'Apuzzo, A. Di Gaspare, P. Di Pietro, I. Lo Vecchio, M. Brahlek, N. Koirala, S. Oh, S. Lupi, *ACS Photonics* **2015**, *2*, 1231.
- [12] M. Autore, F. D'Apuzzo, A. Di Gaspare, V. Giliberti, O. Limaj, P. Roy, M. Brahlek, N. Koirala, S. Oh, F. J. García de Abajo, S. Lupi, *Adv. Opt. Mater.* **2015**, *3*, 1257.
- [13] A. M. Dubrovkin, J. Yin, G. Adamo, Y. Kiasat, B. Qiang, Q. J. Wang, C. Soci, L. Wang, N. I. Zheludev, in *Conf. on Lasers and Electro-Optics*, OSA Publishing, Washington, DC **2016**, DOI: 10.1364/CLEO_QELS.2016.FW4B.3.
- [14] B. Xia, P. Ren, A. Sulaev, P. Liu, S. Q. Shen, L. Wang, *Phys. Rev. B* **2013**, *87*, 085442.
- [15] T. Arakane, T. Sato, S. Souma, K. Kosaka, K. Nakayama, M. Komatsu, T. Takahashi, Z. Ren, K. Segawa, Y. Ando, *Nat. Commun.* **2012**, *3*, 636.
- [16] C. S. Tang, B. Xia, X. Zou, S. Chen, H. W. Ou, L. Wang, A. Rusydi, J. X. Zhu, E. E. M. Chia, *Sci. Rep.* **2013**, *3*, 3513.
- [17] A. M. Dubrovkin, J. Tao, X. C. Yu, N. I. Zheludev, Q. J. Wang, *Sci. Rep.* **2015**, *5*, 09837.
- [18] T. G. Habteyes, *J. Phys. Chem. C* **2014**, *118*, 9119.
- [19] N. Ocelic, A. Huber, R. Hillenbrand, *Appl. Phys. Lett.* **2006**, *89*, 101124.
- [20] M. Schnell, A. García-Etxarri, A. J. Huber, K. Crozier, J. Aizpurua, R. Hillenbrand, *Nat. Photonics* **2009**, *3*, 287.
- [21] L. Wu, W.-K. Tse, M. Brahlek, C. M. Morris, R. Valdés Aguilar, N. Koirala, S. Oh, N. P. Armitage, *Phys. Rev. Lett.* **2015**, *115*, 217602.
- [22] G. Jellison, F. Modine, *Appl. Phys. Lett.* **1996**, *69*, 371.
- [23] S. C. Liou, M. W. Chu, R. Sankar, F. T. Huang, G. J. Shu, F. C. Chou, C. H. Chen, *Phys. Rev. B* **2013**, *87*, 085126.
- [24] T. G. Habteyes, I. Staude, K. E. Chong, J. Dominguez, M. Decker, A. Miroshnichenko, Yu. Kivshar, I. Brener, *ACS Photonics* **2014**, *1*, 794.
- [25] A. M. Dubrovkin, G. Adamo, A. Sulaev, Q. J. Wang, L. Wang, N. I. Zheludev, in *Conf. on Lasers and Electro-Optics*, OSA Publishing, Washington, DC **2015**, EH-2.1.